ADHESION OF AN AXISYMMETRIC ELASTIC BODY: RANGES OF VALIDITY OF MONOMIAL APPROXIMATIONS AND A TRANSITION MODEL

A Thesis Presented

By

Fouad Oweiss

to

The Department of Mechanical and Industrial Engineering

in partial fulfillment of the requirements
for the degree of

Master of Science

in the field of

Mechanical Engineering

Northeastern University
Boston, Massachusetts

December 2015

ABSTRACT

The adhesion forces between two bodies in contact were experimentally observed by Roberts (1968) and Kendall (1969). In these experiments it was noted that the contact areas at low loads were considerably larger than those predicted by Hertz theory. Several models were then introduced to add the adhesion effect to the Hertz model, such as the Johnson-Kendall-Roberts (JKR) model, the Derjaguin-Muller-Toporov (DMT) model and the Maugis model. The Maugis model also offers a transition between the JKR and DMT theories. These models were developed for axisymmetric elastic bodies, with ideal spherical surface profiles, which can be approximated by a single second-order term. Later, Zheng et al.(2007) developed a model that investigated the adhesion of axisymmetric elastic bodies whose surface profiles are ideally approximated by a single n-th order term. Since an actual surface profile may not be exactly described by a single paraboloid or a single higher-order term, it may not be obvious which model is more suitable to use. In this investigation, surface geometries of contacting bodies are approximated by a combination of second- and fourth-order terms and a transition region is established. It is shown that the need for using the transition model not only depends on the geometry of contacting bodies, but also on their material properties.

Keywords: **Adhesion:** Contact, Forces; **Contact:** Elastic; **Model:** Analytical

TABLE OF CONTENTS

Introduction

The elastic contact with adhesion of spherical elastic bodies (whose surface profiles are approximated by a single second-order term) was investigated by Johnson et al. (JKR model) [1] and Derjaguin et al. (DMT model) [2]. Both models add to the Hertz contact model the effect of the Dupré energy of adhesion w, which is defined as the work per unit area needed for the reversible, isothermal separation of two solids. This quantity, also known as the work of adhesion, is given by $w = \gamma_1 + \gamma_2 - \gamma_{12}$, where $\gamma_1$and γ_2 are the surface energies of the two bodies in contact and γ_{12} is the interfacial energy. If the bodies are identical then, $w = 2\gamma$. The JKR model adds the adhesion effect by minimizing the total potential energy which includes the Dupré energy of adhesion, giving a pull-off force of $\frac{3}{2}\pi wR$. The DMT model adds the adhesive stresses outside the contact region while maintaining the Hertz stress distribution inside the contact area, thereby obtaining a pull-off force of $2\pi wR$.

Using the Dugdale model from fracture mechanics, Maugis introduced a model (also known as the M-D model) [3] which demonstrates a continuous transition between the JKR and DMT theories based on a parameter λ that is closely related to the Tabor parameter μ [4]. The Tabor parameter is a measure of the ratio of the elastic deformation to the range of surface forces. The Maugis parameter can be expressed in terms of Tabor parameter as $\lambda \cong 1.16\mu$ Maugis showed that, as $\lambda \to 0$, the DMT model is applicable whereas when $\lambda \to \infty$ the JKR model is called for. For practical purposes λ less than about 0.1 is DMT and λ greater than about 3 is JKR.

Although the three models mentioned above assume that the bodies in contact are spherical, their surface geometries are in fact approximated by a single second-order term.

In their research on the friction force between an atomic force microscope (AFM) tip and a nominally flat surface, Carpick et al. introduced an extended JKR model applicable to axisymmetric elastic bodies in contact with a surface profile described by a single n-th order term, i.e. Cr^n [5, 6]. Later, Zheng et al. developed an analytical model to extend the M-D theory to asperities with such power-law geometries, called the M-D-n model [7]. Grierson et al. then performed a finite element analysis and experimental measurements which agreed well with the analytical model [8].

Some questions naturally arise in deciding whether to use a second- or higher-order approximation of a surface profile. For example, if the real surface profile is "exactly" either a 2^{nd}-order or 4^{th}-order shape then it is clear which shape to use in calculating the pull-off force, the force vs. the contact area, and the force vs. the penetration. However, a realistic shape could no doubt be approximated to different degrees of accuracy by either a 2^{nd}-order or a 4^{th}-order shape. The choice of which approximation to use is expected to depend upon how close the actual profile is to each of these shapes, but does it also depend upon a parameter involving the material properties? Furthermore, under what conditions does the shape need to be described by more than one term, *i.e.* a combination of a 2^{nd}-order term and a 4^{th}-order order term? Another issue is the choice of using the JKR and its extended model as opposed to the more complicated Maugis and its extended model. For a pure 2^{nd}-order surface profile these regimes are reasonably clear. However do these regimes differ for a two-term approximation? By extending JKR and M-D models to a surface profile with two terms, we hope to answer these questions.

JKR Model Extension for Two Terms

A. Problem Formulation:

If a pressure distribution is applied to a circular region of an elastic half space of radius a, a closed-form solution for the normal component of surface displacement can be found. Consider a cylindrical coordinate system (r, θ, z) and apply on $z = 0$ the pressure distribution given by

$$p(r) = p_m \left(1 - \frac{r^2}{a^2}\right)^n \qquad r < a \tag{1}$$

where the maximum contact pressure is p_m, which occurs at $r = 0$.

Following the procedure of Johnson [9] and referring to Figure 1, the displacement of the surface at point B can be found using a local polar coordinate system (s, ϕ) with origin at point B. At a distance s from B, the pressure $p(s, \phi)$ that acts on a small element of area corresponds to a force with magnitude $p(s, \phi)\ s\ ds\, d\phi$. The displacement at B resulting from the pressure distributed on the whole area is then

$$u_z = \frac{1-\nu^2}{\pi E} \iint_s p(s, \phi)\ ds\, d\phi \tag{2}$$

where ν is Poisson's ratio and E is Young's modulus.

The resultant force P is obtained by integration of the pressure over the circular region

$$P = \int_0^a 2\pi r\ p(r) dr \tag{3}$$

The value of the exponent n in the above pressure distribution depends on the surface profile of the elastic bodies in contact. For example $n = \frac{1}{2}$ represents the pressure distribution between two spherical elastic solids in frictionless contact without adhesion as obtained by Hertz (1882) i.e.

$$p(r) = p_1\left(1 - \frac{r^2}{a^2}\right)^{\frac{1}{2}} \qquad r < a \tag{4}$$

where $p_1$is the maximum contact stress and can be written in terms of the resultant force P_1 as

$$p_1 = \frac{3P_1}{2\pi a^2} \tag{5}$$

The displacement expressed in terms of the resultant force P_1 is

$$u_z(r,0) = \frac{3P_1}{8E^* a}\left(2 - \frac{r^2}{a^2}\right) \qquad 0 < r < a \tag{6}$$

$$u_z(r,0) = \frac{3P_1}{4\pi a E^*}\left[\left(\left(2 - \frac{r^2}{a^2}\right)\sin^{-1}\frac{a}{r}\right) + \left(\sqrt{\frac{r^2}{a^2} - 1}\right)\right] \qquad r > a \tag{7}$$

where E^* is the composite Young's modulus defined by

$$\frac{1}{E^*} = \frac{1-\nu_1^2}{E_1} + \frac{1-\nu_2^2}{E_2} \tag{8}$$

where E_1 and E_2 are the elastic Young's moduli of elastic bodies 1 and 2 respectively, and ν_1 and ν_2 are the Poisson's ratios of bodies 1 and 2 respectively.

A pressure distribution in which $n = -\frac{1}{2}$ results in a uniform normal displacement of the circular region ($r < a$) and corresponds to the pressure exerted by a flat-ended, frictionless, rigid punch pressed against an elastic half space with contact radius a (Johnson, 1985). The contact pressure at the center of the circular region, p_2, can be expressed in terms of the resultant force P_2 as

$$p_2 = \frac{P_2}{2\pi a^2} \tag{9}$$

In this case, the displacement at the surface is

$$u_z(r,0) = \frac{P_2}{2E^* a} \qquad 0 < r < a \tag{10}$$

$$u_z(r,0) = \frac{P_2}{\pi a E^*} \sin^{-1}\frac{a}{r} \qquad r > a \tag{11}$$

By using the fracture mechanics concept of the stress intensity factor K_I at the edge of the circular region, the force needed to separate the punch from the half-space may be obtained as a function of the Dupré energy of adhesion w

$$K_I = \lim_{r \to a} p(r)\sqrt{2\pi(a-r)} \tag{12}$$

By setting K_I equal to its critical value

$$-\frac{P_2}{2\sqrt{\pi a^3}} = \sqrt{2wE^*} \tag{13}$$

is obtained. The displacement inside the circular region is therefore:

$$u_z(r,0) = -\sqrt{\frac{2\pi w a}{E^*}} \qquad 0 < r < a \tag{14}$$

If the exponent value n of the pressure distribution is equal to $\frac{3}{2}$, the maximum contact pressure p_3 and a resultant force P_3 are related by

$$p_3 = \frac{5P_3}{2\pi a^2} \tag{15}$$

The corresponding displacements are

$$u_z(r,0) = \frac{15P_3}{16aE^*}\left(1 - \frac{r^2}{a^2} + \frac{3}{8}\frac{r^4}{a^4}\right) \qquad 0 < r < a \tag{16}$$

and

$$u_z(r,0) = \frac{15P_3}{8\pi aE^*}\left[\left((1-\frac{r^2}{a^2}+\frac{3}{8}\frac{r^4}{a^4})\sin^{-1}\frac{a}{r}\right)+\left(\sqrt{\frac{r^2}{a^2}-1}\right)\left(\frac{3}{4}-\frac{3}{8}\frac{r^2}{a^2}\right)\right],\ r>a \quad (17)$$

A superposition of these three pressure distributions results in the following surface displacements

$$\text{for } 0<r<a$$

$$u_z(r,0) = \left[-\sqrt{\frac{2\pi wa}{E^*}}+\frac{3P_1}{4E^*a}+\frac{15P_3}{16E^*a}\right]-\left[\frac{3P_1}{8E^*a^3}+\frac{15P_3}{16E^*a^3}\right]r^2+\left[\frac{45P_3}{128E^*a^5}\right]r^4 \quad (18)$$

and

$$\text{for } r>a$$

$$u_z(r,0) = \frac{1}{\pi aE^*}\left[\begin{array}{c}\left[\left(\sin^{-1}\frac{a}{r}\right)\left(P_2+\frac{3}{4}P_1\left(2-\frac{r^2}{a^2}\right)+\frac{15}{8}P_3\left(1-\frac{r^2}{a^2}+\frac{3}{8}\frac{r^4}{a^4}\right)\right)\right]\\+\left[\left(\sqrt{\frac{r^2}{a^2}-1}\right)\left(\frac{3}{4}P_1+\frac{15}{8}P_3\left(\frac{3}{4}-\frac{3}{8}\frac{r^2}{a^2}\right)\right)\right]\end{array}\right] \quad (19)$$

Now if the surface profile of the elastic body in contact is described by a combination of a 2nd- and a 4th-order terms, then the surface displacement is given by

$$u_z(r,0) = \delta - \frac{r^2}{2R}\left(1+\varepsilon\frac{r^2}{R^2}\right) \qquad 0<r<a \quad (20)$$

where δ is the interference and R is the composite radius of curvature expressed as

$$\frac{1}{R} = \frac{1}{R_1}+\frac{1}{R_2} \quad (21)$$

where R_1 and R_2 are the radii of curvatures of bodies 1 and 2 respectively. By matching the terms in Eqn. (18) to Eqn. (20)

$$P_1 = \frac{4E^* a^3}{3R}\left(1 + \frac{8}{3}\varepsilon\left(\frac{a}{R}\right)^2\right) \tag{22}$$

$$P_2 = -\sqrt{8\pi w E^* a^3} \tag{23}$$

$$P_3 = -\frac{64\varepsilon E^* a^5}{45R^3} \tag{24}$$

are obtained. The total resultant force P is obtained by summing these three forces and is given by

$$P = -\sqrt{8\pi w E^* a^3} + \frac{4E^* a^3}{3R}\left(1 + \frac{8\varepsilon}{5R^2}a^2\right) \tag{25}$$

whereas the total interference is

$$\delta = \left[-\sqrt{\frac{2\pi w a}{E^*}} + \frac{a^2}{R}\left(1 + \frac{4\varepsilon a^4}{3R^3}\right)\right] \tag{26}$$

Both of the above equations can be simplified by introducing non-dimensional parameters given by

$$\bar{a} = \left(\frac{4E^*}{3\pi w R^2}\right)^{\frac{1}{3}} a \tag{27}$$

$$\bar{P} = \frac{P}{\pi w R} \tag{28}$$

$$\varepsilon' = \varepsilon\frac{2}{5}\left(\frac{6\pi w}{E^* R}\right)^{\frac{2}{3}} \tag{29}$$

$$\bar{\delta} = \left(\frac{16E^{*2}}{9\pi^2 w^2 R}\right)^{\frac{1}{3}} \delta \tag{30}$$

The non-dimensional load and non-dimensional approach may now be written as

$$\bar{P} = -\sqrt{6\bar{a}^3} + \bar{a}^3(1 + \varepsilon'\bar{a}^2) \tag{31}$$

$$\bar{\delta} = -\sqrt{\frac{8}{3}\bar{a}} + \bar{a}^2\left(1 + \frac{5}{6}\varepsilon'\bar{a}^2\right) \tag{32}$$

In summary Eqns. (31) and (32) can be used to relate the dimensionless force to contact radius and approach for various values of ε'.

B. Results and Discussion

In Figure 2, the dimensionless contact radius vs. the dimensionless load is plotted for different values of ε'. Note that ε' as defined by Eqn. (29) depends not only on the relative magnitude of the fourth-order term compared to the second-order term, but it also depends on *w/E*R*. The solid lines in Fig. 2 represent the results for a surface profile described by a combination of 2nd- and 4th-order terms, whereas the dashed lines represent a pure 4th-order surface profile. It is noted that for a given positive (compressive) load, the resulting contact radius decreases as the weight of the 4th-order term increases compared to the 2nd-order term (i.e. an increase of ε'). For ε' as low as about 0.05 (not shown), the effect of the 4th-order term is important. Also it is not until ε' is as large as about 10 that the pure 4th-order description is accurate. Thus the range $0.05 < \varepsilon' < 10$ describes the transition in which a two-term approximation is needed.

In Figure 3, the dimensionless force vs. the dimensionless approach (interference) is plotted for different values of ε'. Again, the solid lines represent a surface profile described by a combination of 2nd- and 4th-order terms, whereas the dashed lines represent a pure 4th-order surface profile. The range $0.05 < \varepsilon' < 10$ still describes the transition region in which a two-term approximation is needed. For a geometry described by two terms, separation of the bodies

in contact (which occurs at the maximum tensile load) is accompanied by a dimensionless negative interference (stretching) ranging from approximately $\bar{\delta} = -0.9$ at $\varepsilon' = 0$ to around $\bar{\delta} = -0.75$ at $\varepsilon' = 10$.

In Figure 4, the dimensionless pull-off force $\bar{P}_{off}$ (i.e. the maximum tensile force) is plotted as a function of ε'. Also shown is the curve-fit equation which is expressed in the form

$$\bar{P}_{off} = 0.7905e^{-0.05618\varepsilon'} + 0.7094e^{-1.39\varepsilon'} \tag{33}$$

The root mean squared error between the curve-fit and the data is about 1.7%, with a maximum error of about 4.8%. It is noted that the results reduce to the original JKR model when $\varepsilon' = 0$.

Maugis Model Extension to Two Terms

A. Problem Formulation

The model introduced by Maugis [3], which was developed for spherical bodies in contact, will now be extended to a combined 2nd- and 4th-order shape. The first step is to determine the solution due to a single term 4th-order shape without adhesion; it corresponds to a summation of pressure distributions with $n = \frac{1}{2}$ and $n = \frac{3}{2}$. This solution will then be superposed onto the Maugis solution in such a manner as to account for the fact that the added pressure distribution changes the displacement in the separation region and hence affects the adhesion condition.

For a pressure distribution given by

$$p(r) = p_1\left(1 - \frac{r^2}{a^2}\right)^{\frac{1}{2}} + p_3\left(1 - \frac{r^2}{a^2}\right)^{\frac{3}{2}} \qquad r < a \tag{34}$$

by using Eqn. (2), the resulting displacement is

$$\text{for} \quad 0 < r < a$$

$$u_z(r,0) = \frac{1}{16aE^*}\left[(12P_1 + 15P_3) - (6P_1 + 15P_3)\frac{r^2}{a^2} + (15P_3)\frac{3}{8}\frac{r^4}{a^4}\right] \tag{35}$$

$$\text{and for} \quad r > a$$

$$u_z(r,0) = \frac{1}{8\pi aE^*}\left[\begin{array}{c}\left[\left(\sin^{-1}\frac{a}{r}\right)\left(6P_1\left(2-\left(\frac{r}{a}\right)^2\right) + 15P_3\left(1-\left(\frac{r}{a}\right)^2 + \frac{3}{8}\left(\frac{r}{a}\right)^4\right)\right)\right] \\ + \left[\left(\sqrt{\left(\frac{r}{a}\right)^2 - 1}\right)\left(6P_1 + 15P_3\left(\frac{3}{4} - \frac{3}{8}\left(\frac{r}{a}\right)^2\right)\right)\right]\end{array}\right] \tag{36}$$

If the surface profile of the elastic body in contact is described by a single 4th-order term, *i.e.*

$$u_z(r,0) = \delta - \varepsilon\frac{r^4}{2R^3} \qquad\qquad 0 < r < a \tag{37}$$

then, by matching Eqns. (35) and (37)

$$P_3 = -\frac{64\varepsilon E^* a^5}{45R^3} \tag{39}$$

$$P_1 = \frac{32\varepsilon E^* a^5}{9R^3} \tag{40}$$

are obtained. The corresponding total load (P_ε) and interference (δ_ε) are given by

$$P_\varepsilon = P_1 + P_3 = \frac{32\varepsilon E^* a^5}{15R^3} \tag{41}$$

$$\delta_\varepsilon = \frac{4\varepsilon a^4}{3R^3} \tag{42}$$

for this pure 4th-order shape without adhesion. The gap resulting from the pressure distribution due to a 4th-order shape becomes

$$[u_{z\varepsilon}] = \frac{4\varepsilon a^4}{3R^3}\left[\left(\frac{2}{\pi}\cos^{-1}\frac{a}{r}\right)\left(\frac{3}{8}\left(\frac{r}{a}\right)^4 - 1\right)\right] + \frac{8\varepsilon a^4}{3\pi R^3}\left[\left(\sqrt{\left(\frac{r}{a}\right)^2 - 1}\right)\left(\frac{1}{4} + \frac{3}{8}\left(\frac{r}{a}\right)^2\right)\right] \quad (43)$$

Now considering the results of Maugis, the relative normal displacement in the separation region for a parabolic shaped profile with a constant adhesive stress (σ_o) is at $r = c$

$$h_o = \frac{a^2}{\pi R}\left[\sqrt{m^2-1} + (m^2-2)\tan^{-1}\sqrt{m^2-1}\right] + \frac{4\sigma_o a}{\pi E^*}\left[(\sqrt{m^2-1}\tan^{-1}\sqrt{m^2-1}) + 1 - m\right] \quad (44)$$

where $m = \frac{c}{a}$. Note that in the Maugis model and its extension a constant adhesive stress is assumed at points in the separation region for which the local separation is less than h_o, where $h_o\sigma_o = w$ defines the value of h_o. Maugis shows that h_o is approximately equal to the atomic equilibrium separation (Z_o) of two half-spaces. The stress due to adhesion is assumed to be a constant σ_o in this region and zero elsewhere.

Thus for the combined 2nd-and 4th-order model, the total air gap $[u_z]$ at $r = c$ can be expressed as:

$$h_o = \left[\left[\frac{a^2(m^2-2)}{\pi R} + \frac{8\varepsilon a^4\left(\frac{3}{8}m^4-1\right)}{3\pi R^3}\right]\tan^{-1}\sqrt{m^2-1}\right] + \left[\left[\frac{a^2}{\pi R} + \frac{2\varepsilon a^4}{3\pi R^3} + \frac{\varepsilon a^4}{\pi R^3}m^2\right]\sqrt{m^2-1}\right] +$$
$$\left[\frac{4\sigma_o a}{\pi E^*}\left[(\sqrt{m^2-1}\tan^{-1}\sqrt{m^2-1}) + 1 - m\right]\right] \quad (45)$$

in which the identity $\cos^{-1}\frac{1}{m} = \tan^{-1}\sqrt{m^2-1}$ has been used,.

Now the Maugis dimensionless parameter is introduced

$$\lambda = \frac{2\sigma_o}{\left(\frac{\pi w K^2}{R}\right)^{\frac{1}{3}}} = \frac{2\sigma_o}{\left(\frac{\pi w\left(\frac{4}{3}E^*\right)^2}{R}\right)^{\frac{1}{3}}} \tag{46}$$

This dimensionless parameter can be related to Tabor parameter, μ as follows:

$$\sigma_o = \frac{w}{0.97\ Z_o} \tag{47}$$

and Eqn. (46) can be rewritten as:

$$\lambda = \left[\frac{8Rw^2}{(0.97)^3\pi\left(\frac{4}{3}\right)^2 E^{*2} {Z_o}^3}\right]^{\frac{1}{3}} \tag{48}$$

The Tabor parameter μ [4] is expressed as:

$$\mu = \left[\frac{Rw^2}{E^{*2} {Z_o}^3}\right]^{\frac{1}{3}} \tag{49}$$

Therefore:

$$\lambda_{Maugis} \cong 1.16\ \mu_{Tabor} \tag{50}$$

Using Eqn. (46), Eqn. (45) becomes

$$\frac{\lambda\bar{a}^2}{2}\left[\left(1 + \frac{5\varepsilon'\bar{a}^2}{8}\left(m^2 + \frac{2}{3}\right)\right)\sqrt{m^2-1} + \left((m^2-2) + \frac{5\varepsilon'\bar{a}^2}{3}\left(\frac{3}{8}m^4 - 1\right)\right)\tan^{-1}\sqrt{m^2-1}\right] +$$

$$\frac{4}{3}\lambda^2\bar{a}\left[\left(\sqrt{m^2-1}\tan^{-1}\sqrt{m^2-1}\right) + 1 - m\right] = 1 \tag{51}$$

which reduces to equation (6.17) in [3] if $\varepsilon' = 0$. Equations (41) and (42) can be rewritten using dimensionless parameters as

$$\bar{P}_{\varepsilon} = \varepsilon' \bar{a}^5 \tag{52}$$

$$\bar{\delta}_{\varepsilon} = \frac{5}{6}\varepsilon' \bar{a}^4 \tag{53}$$

The total dimensionless load can be obtained by adding equation (52) to the dimensionless load obtained by Maugis [3] (equation 6.18) and is

$$\bar{P} = \varepsilon' \bar{a}^5 + \bar{a}^3 - \lambda \bar{a}^2 \left[\sqrt{m^2 - 1} + m^2 \tan^{-1} \sqrt{m^2 - 1}\right] \tag{54}$$

The dimensionless approach given by Eqn. (53) can be added to Eqn. 6.19 in [3] to give the total dimensionless approach:

$$\bar{\delta} = \frac{5}{6}\varepsilon' \bar{a}^4 + \bar{a}^2 - \frac{4}{3}\bar{a}\lambda\sqrt{m^2 - 1} \tag{55}$$

It is noted that when $\varepsilon' = 0$ Eqns. (54) and (55) reduce to the original equations obtained by Maugis.

To obtain the values of dimensionless load and the dimensionless approach relevant to a pure 4th-order shape, the surface profile of the elastic body in contact is assumed so as to suppress the second order term when superposed to the original M-D model, i.e.

$$u_z(r, 0) = \delta + \frac{r^2}{2R} - \varepsilon \frac{r^4}{2R^3} \qquad 0 < r < a \tag{56}$$

Then by matching Eqns. (35) and (56)

$$P_3 = -\frac{64\varepsilon E^* a^5}{45R^3} \tag{57}$$

$$P_1 = \frac{32\varepsilon E^* a^5}{9R^3} - \frac{4a^3 E^*}{3R} \tag{58}$$

are obtained. The corresponding total load (P') and interference (δ') without adhesion are given by

$$P' = P_1 + P_3 = \frac{32\varepsilon E^* a^5}{15R^3} - \frac{4a^3 E^*}{3R} \tag{59}$$

$$\delta' = \frac{4\varepsilon a^4}{3R^3} - \frac{a^2}{R} \tag{60}$$

for the shape in Eqn. (56) which can be written in dimensionless form as

$$\bar{P}' = \varepsilon' \bar{a}^5 - \bar{a}^3 \tag{61}$$

$$\bar{\delta}' = \frac{5}{6}\varepsilon' \bar{a}^4 - \bar{a}^2 \tag{62}$$

The gap resulting from the pressure distribution due to the shape in Eqn. (56) becomes

$$[u_z'] = \frac{\varepsilon a^4}{2R^3}\left[\left(\frac{2}{\pi}\cos^{-1}\frac{a}{r}\right)\left(\left(\frac{r}{a}\right)^4 - \frac{8}{3}\right)\right] + \frac{\varepsilon a^4}{\pi R^3}\left[\left(\sqrt{\left(\frac{r}{a}\right)^2 - 1}\right)\left(\left(\frac{r}{a}\right)^2 + \frac{2}{3}\right)\right] \tag{63}$$

By adding Eqns. (44) and (63), the total air gap at $r = c$ can be expressed as

$$h_o = \left[\left[\frac{\varepsilon a^4}{\pi R^3}\left(m^4 - \frac{8}{3}\right)\right]\tan^{-1}\sqrt{m^2 - 1}\right] + \left[\frac{\varepsilon a^4}{\pi R^3}\left(m^2 + \frac{2}{3}\right)\sqrt{m^2 - 1}\right]$$

$$+ \left[\frac{4\sigma_o a}{\pi E^*}\left[\left(\sqrt{m^2 - 1}\tan^{-1}\sqrt{m^2 - 1}\right) + 1 - m\right]\right] \tag{64}$$

Using Maugis dimensionless parameter from Eqn. (46), Eqn. (64) becomes

$$\frac{5\varepsilon'\lambda\bar{a}^4}{16}\left[\left(m^2+\frac{2}{3}\right)\sqrt{m^2-1}+\left(m^4-\frac{8}{3}\right)\tan^{-1}\sqrt{m^2-1}\right]+$$

$$\frac{4}{3}\lambda^2\bar{a}\left[(\sqrt{m^2-1}\tan^{-1}\sqrt{m^2-1})+1-m\right]=1 \quad (65)$$

By adding the dimensionless load and dimensionless approach obtained by Maugis, the total dimensionless load for a pure 4th-order shape with adhesion becomes

$$\bar{P}=\varepsilon'\bar{a}^5-\lambda\bar{a}^2\left[\sqrt{m^2-1}+m^2\tan^{-1}\sqrt{m^2-1}\right] \quad (66)$$

and the total dimensionless approach for a pure 4th-order shape with adhesion is given by

$$\bar{\delta}=\frac{5}{6}\varepsilon'\bar{a}^4-\frac{4}{3}\bar{a}\lambda\sqrt{m^2-1} \quad (67)$$

B. Results and Discussion

In Figures 5 through 8, the dimensionless contact radius is plotted vs. the dimensionless load for $\lambda = 0.5\,, 1, 1.5\ and\ 3$ respectively. Also, the dimensionless load is plotted vs. the dimensionless approach in Figures 9 through 12 at $\lambda = 0.5\,, 1, 1.5\ and\ 3$ respectively. Based on these results, a single 4th-order term can be used to describe the surface profile of an elastic body when $\varepsilon' > 10$, while a single 2nd-order term may be used if $\varepsilon' < 0.05$. In the transition range where $0.05 < \varepsilon' < 10$, the surface profile should be described by two terms.

Figure 13 highlights the decrease in the pull-off force as ε' increases for a variety of λ. At large values of ε' (Fig. 13a) the trend is clear that greater values of λ lead to greater values of the pull-off force. However for smaller values of ε' (Fig. 13b) the trend is much more complicated. The variation of the dimensionless contact radius at pull-off vs. ε' is shown in Figure 14 for various values of λ. Finally, Figure 15 shows the dimensionless approach at pull-off (stretching, since it is negative) vs. as ε' for different values of λ.

Conclusions

The extension of the JKR and Maugis models to two terms has been accomplished. The results demonstrate the conditions under which using a single 2nd-order term, a single 4th-order term, or the two-term approximation is needed. This determination is based upon a parameter ε' which represents a combination of the relative weight of the 4th-order term compared to the 2nd-order term and also on the ratio of the work of adhesion to the product of the composite Young's modulus and the radius of curvature of the body. From these results, the surface profile of an elastic body can be approximated to a single 2nd-order form if ε' is less than about 0.05, whereas a single 4th-order term approximation is applicable for ε' greater than about 10. Therefore the range $0.05 < \varepsilon' < 10$ is the transition regime in which a two-term approximation is called for.

REFERENCES

[1] Johnson, K.L., Kendall, K., and Roberts, A.D., 1971, "Surface Energy and the Contact of Elastic Solids," *Proceedings of the Royal Society of London,* **A324**, pp. 301-313.

[2] Derjaguin, B.V., Muller, V.M., and Toporov, Y.P., 1975, "Effect of Contact Deformations on the Adhesion of Particles," *Journal of Colloid and Interface Science,* **53**, pp. 314-326.

[3] Maugis, D., 1992, "Adhesion of Spheres: The JKR-DMT Transition Using a Dugdale Model," *Journal of Colloid and Interface Science,* **150**, pp. 243-269.

[4] Tabor, D., 1976, "Surface Forces and Surface Interactions," *Journal of Colloid and Interface Science*, **58**, pp. 2-13.

[5] Carpick, R.W., Agraït, N., Ogletree, D.F., Salmeron, M., 1996a, "Measurement of interfacial shear (friction) with an ultrahigh vacuum atomic force microscope," *Journal of Vacuum Science and Technology B*, **14**, pp.1289-1295.

[6] Carpick, R.W., Agraït, N., Ogletree, D.F., Salmeron, M., 1996b, "Erratum: Measurement of interfacial shear (friction) with an ultrahigh vacuum atomic force microscope," *Journal of Vacuum Science and Technology B*, **14**, pp.1289-1295.

[7] Zheng, Z., Yu, J., 2007, "Using the Dugdale approximation to match a specific interaction in the adhesive contact of elastic objects," *Journal of Colloid and Interface Science*, **310**, pp. 27-34.

[8] Grierson, D.S., Liu, J., Carpick, R.W., Turner, K.T., 2013, "Adhesion of nanoscale asperities with power-law profiles", *Journal of the Mechanics and Physics of Solids*, **61**, pp. 597-610

[9] Johnson, K.L., 1985, "Contact mechanics," pp. 56-62

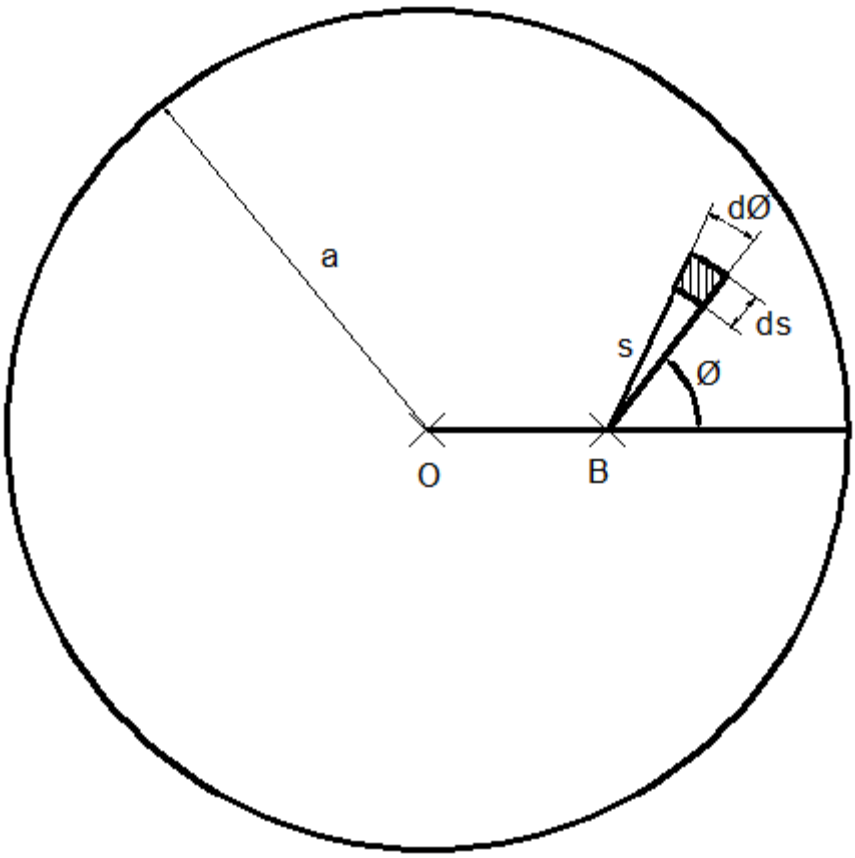

Figure 1. Schematic of axisymmetric elastic body with center O showing point B, at distance r from the center, used to calculate vertical displacement u_z.

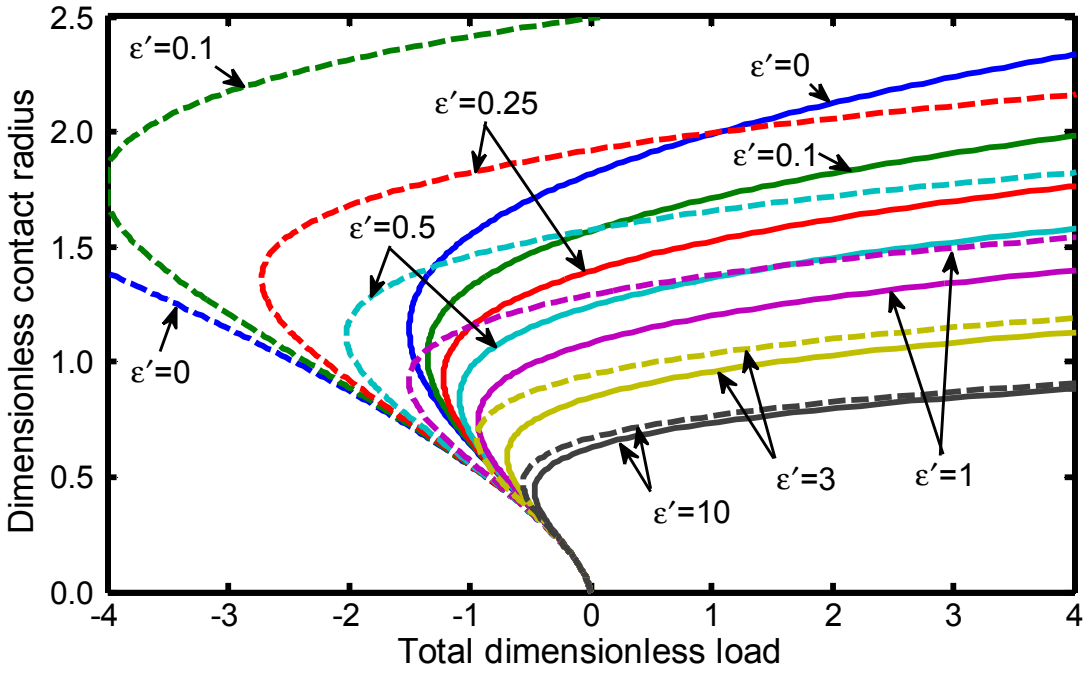

Figure 2.The dimensionless contact radius vs dimensionless load for different values of ε'. The solid lines represent a surface profile described by a combination of a 2nd- and 4th-order terms, whereas the dashed lines represent a surface profile described by a single 4th-order term.

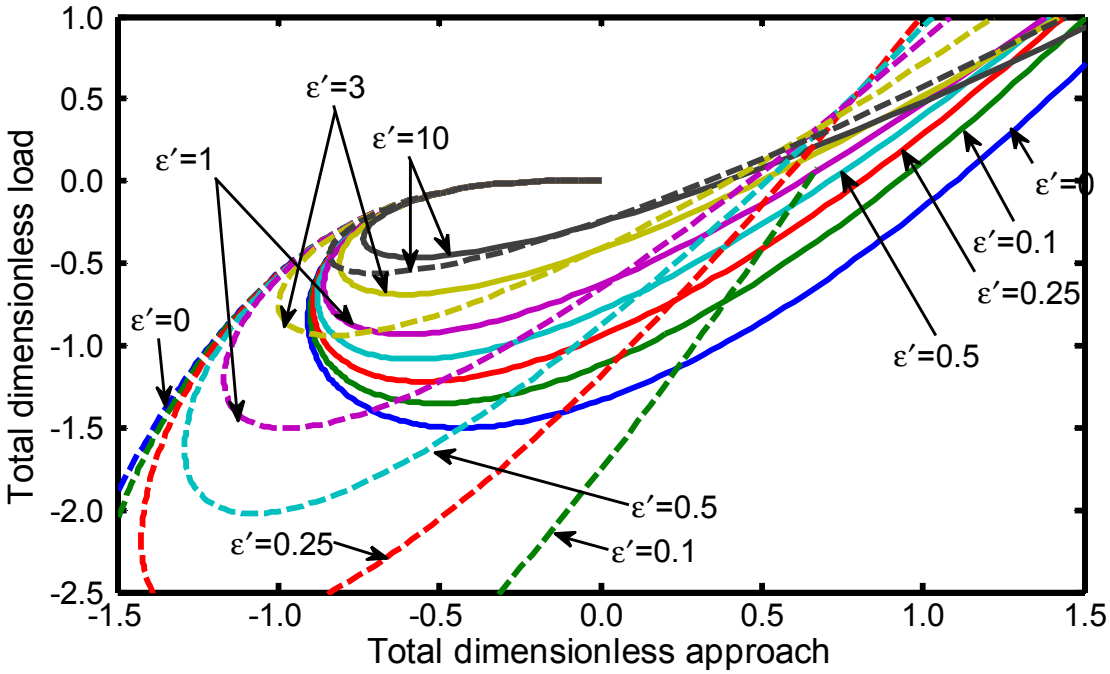

Figure 3. The dimensionless load vs dimensionless approach for different values of ε'.The solid lines represent a surface profile described by a combination of a 2nd- and 4th-order terms, whereas the dashed lines represent a surface profile described by a single 4th-order term.

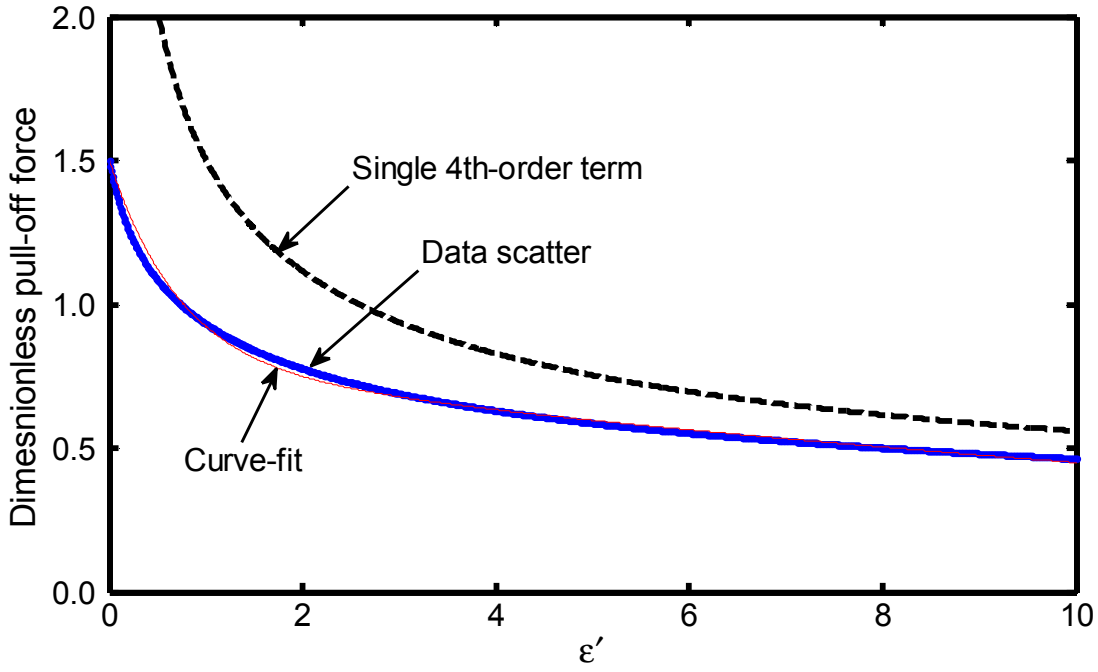

Figure 4. Data scatter and curve-fit for the variation in dimensionless pull-off force with ε' for a surface profile described by a combination of 2nd- and 4th-order terms. The dashed curve represents the pull-off force for a surface profile described by a single 4th-order term.

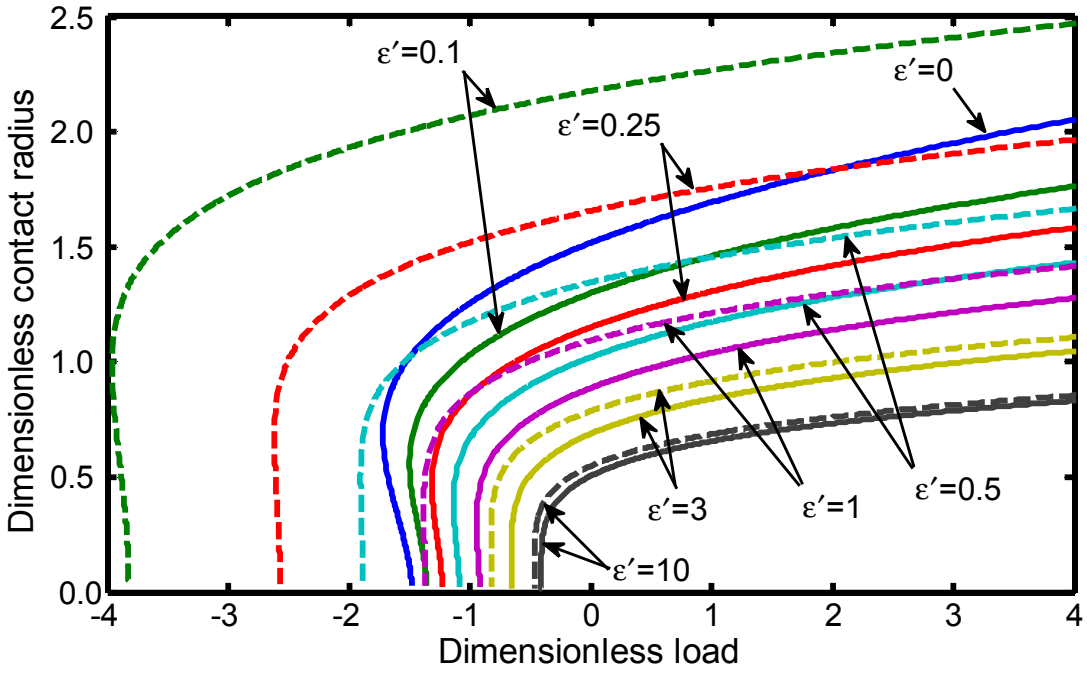

Figure 5 Dimensionless contact radius vs. dimensionless load at $\lambda = 0.5$ at different values of ε'. The solid lines represent a surface profile described by a combination of a 2nd- and 4th-order terms, whereas the dashed lines represent a surface profile described by a single 4th-order term.

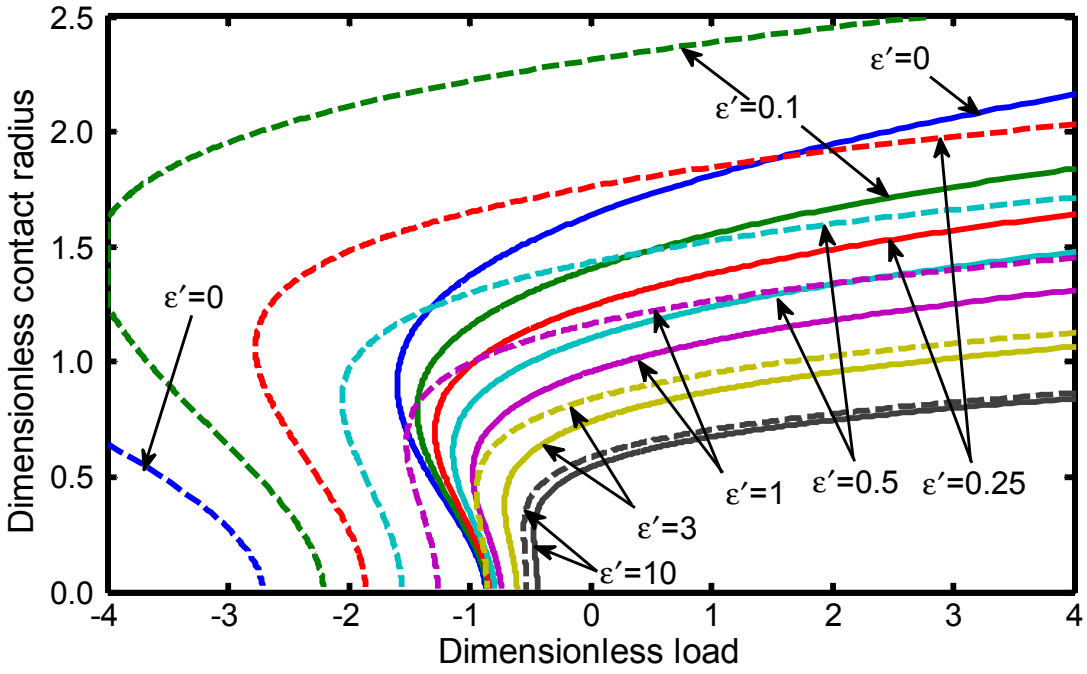

Figure 6 Dimensionless contact radius vs. dimensionless load at $\lambda = 1$ at different values of ε'. The solid lines represent a surface profile described by a combination of a 2nd- and 4th-order terms, whereas the dashed lines represent a surface profile described by a single 4th-order term.

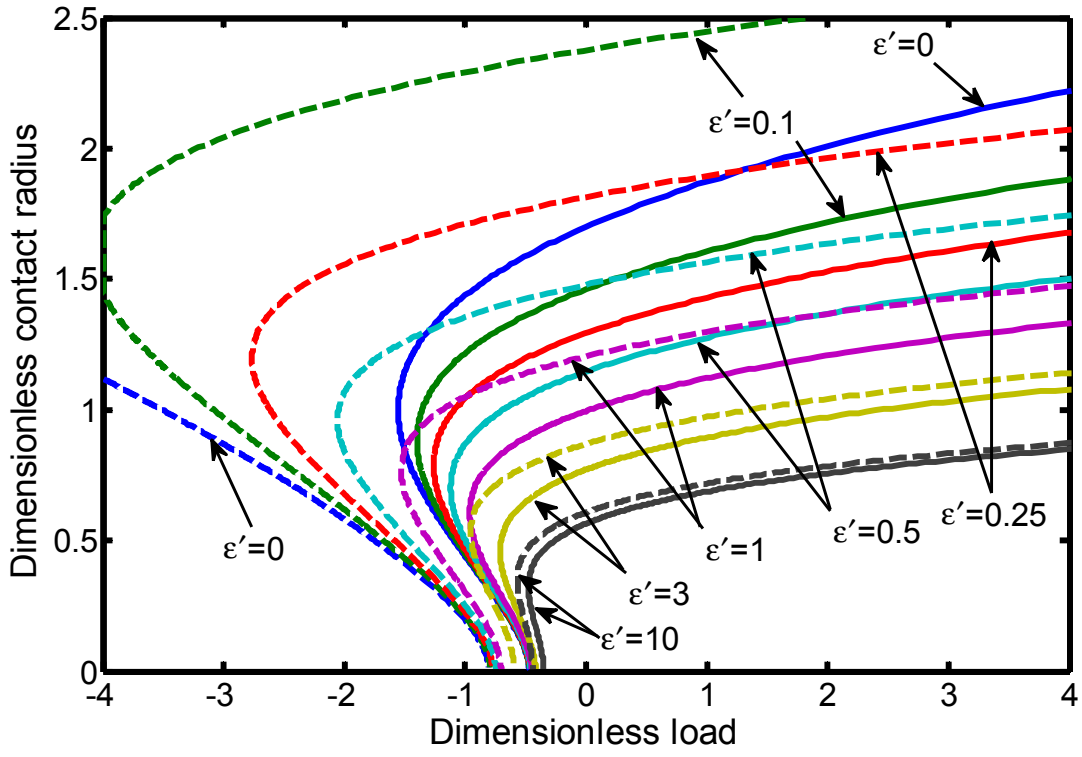

Figure 7 Dimensionless contact radius vs. dimensionless load at $\lambda = 1.5$ at different values of ε'. The solid lines represent a surface profile described by a combination of a 2nd- and 4th-order terms, whereas the dashed lines represent a surface profile described by a single 4th-order term.

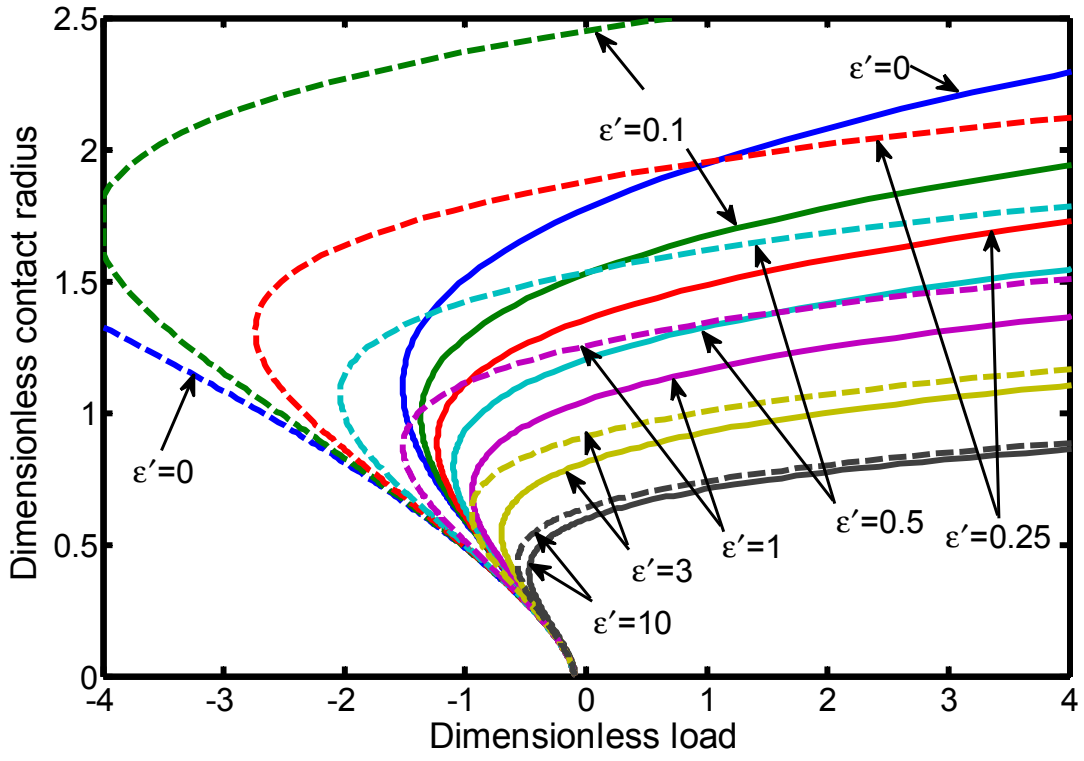

Figure 8 Dimensionless contact radius vs. dimensionless load at $\lambda = 3$ at different values of ε'. The solid lines represent a surface profile described by a combination of a 2nd- and 4th-order terms, whereas the dashed lines represent a surface profile described by a single 4th-order term.

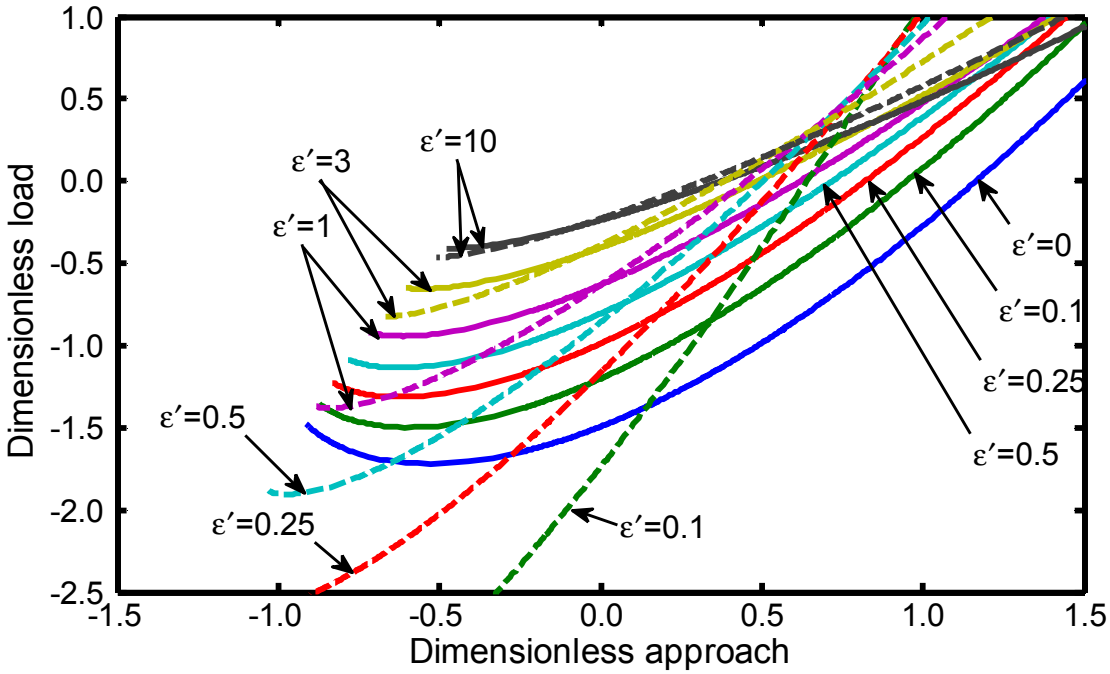

Figure 9 Dimensionless load vs. dimensionless approach at $\lambda = 0.5$ at different values of ε'. The solid lines represent a surface profile described by a combination of a 2nd- and 4th-order terms, whereas the dashed lines represent a surface profile described by a single 4th-order term.

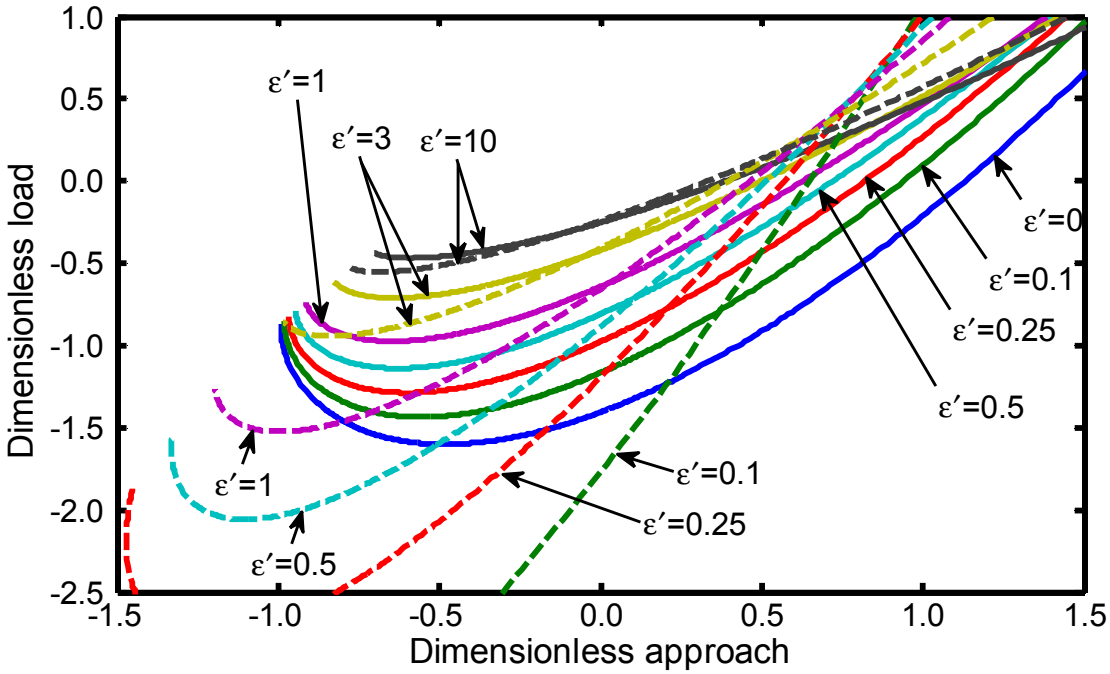

Figure 10 Dimensionless load vs. dimensionless approach at $\lambda = 1$ at different values of ε'. The solid lines represent a surface profile described by a combination of a 2nd- and 4th-order terms, whereas the dashed lines represent a surface profile described by a single 4th-order term.

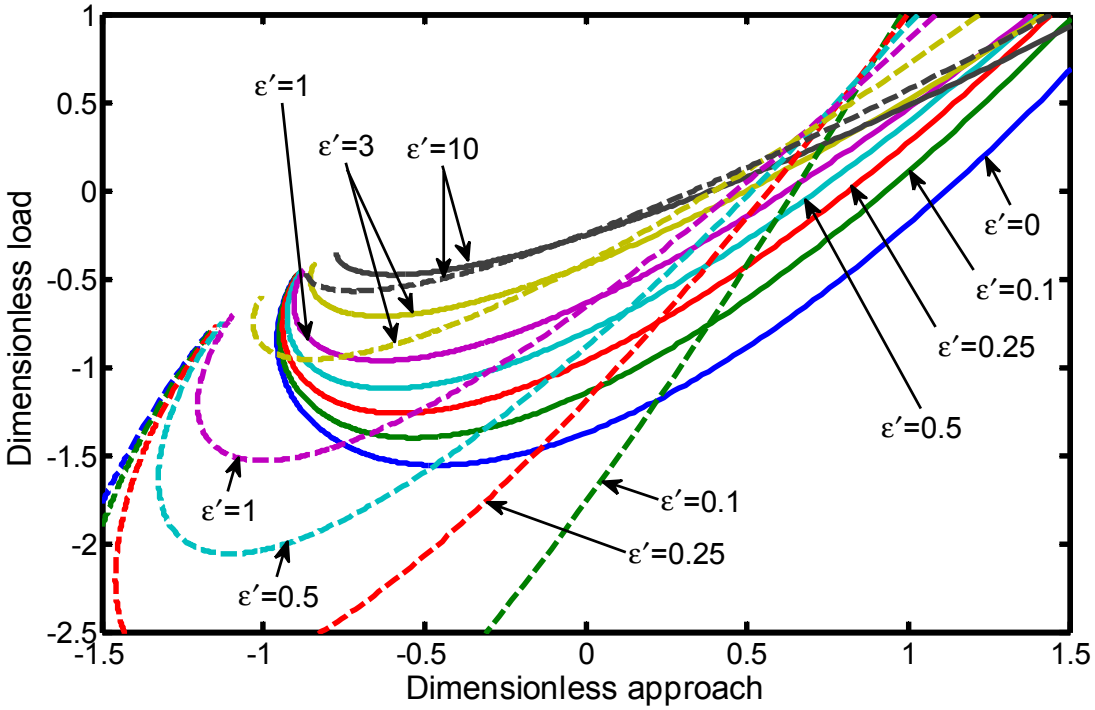

Figure 11 Dimensionless load vs. dimensionless approach at $\lambda = 1.5$ at different values of ε'. The solid lines represent a surface profile described by a combination of a 2nd- and 4th-order terms, whereas the dashed lines represent a surface profile described by a single 4th-order term.

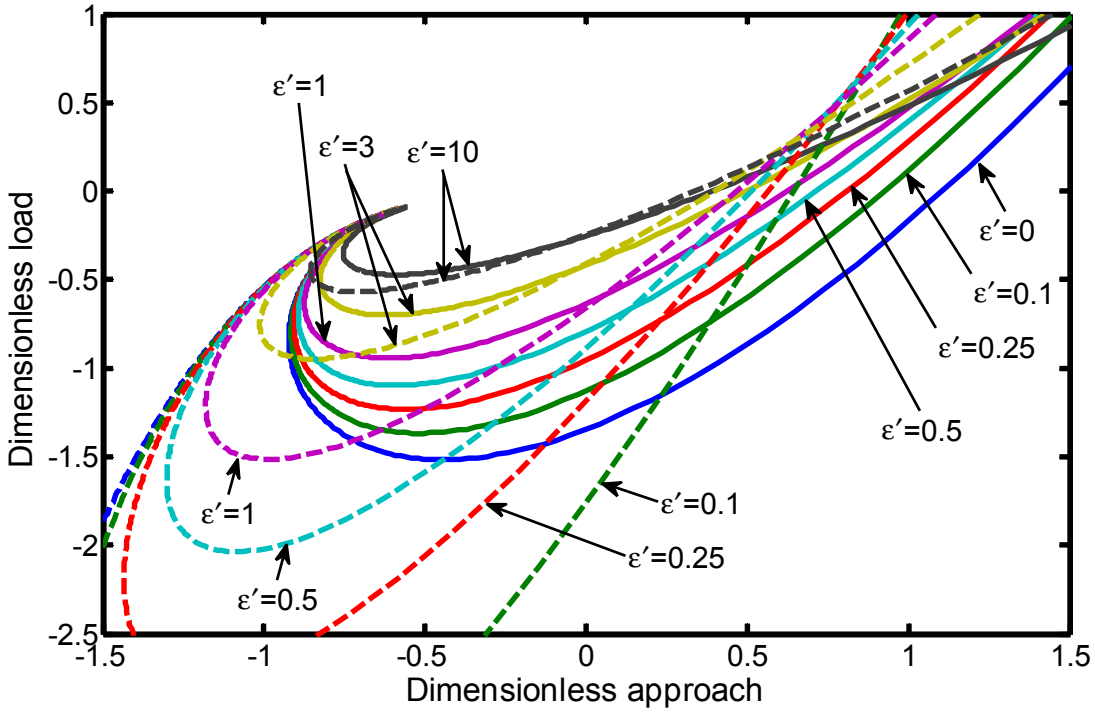

Figure 12 Dimensionless load vs. dimensionless approach at $\lambda = 3$ at different values of ε'. The solid lines represent a surface profile described by a combination of a 2nd- and 4th-order terms, whereas the dashed lines represent a surface profile described by a single 4th-order term.

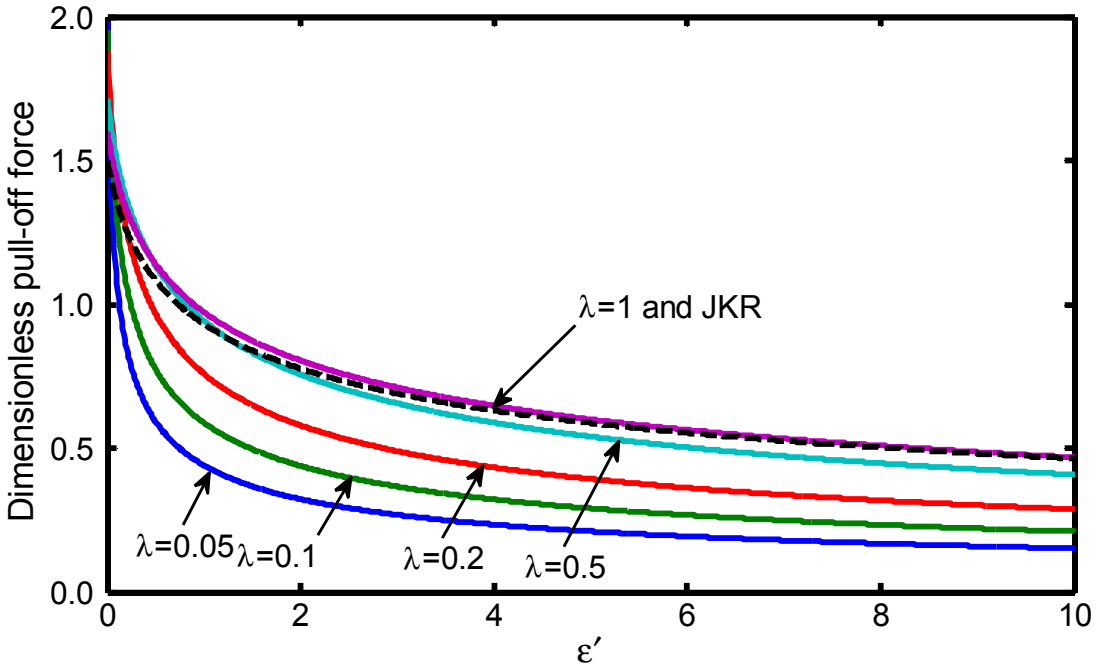

Figure 13a

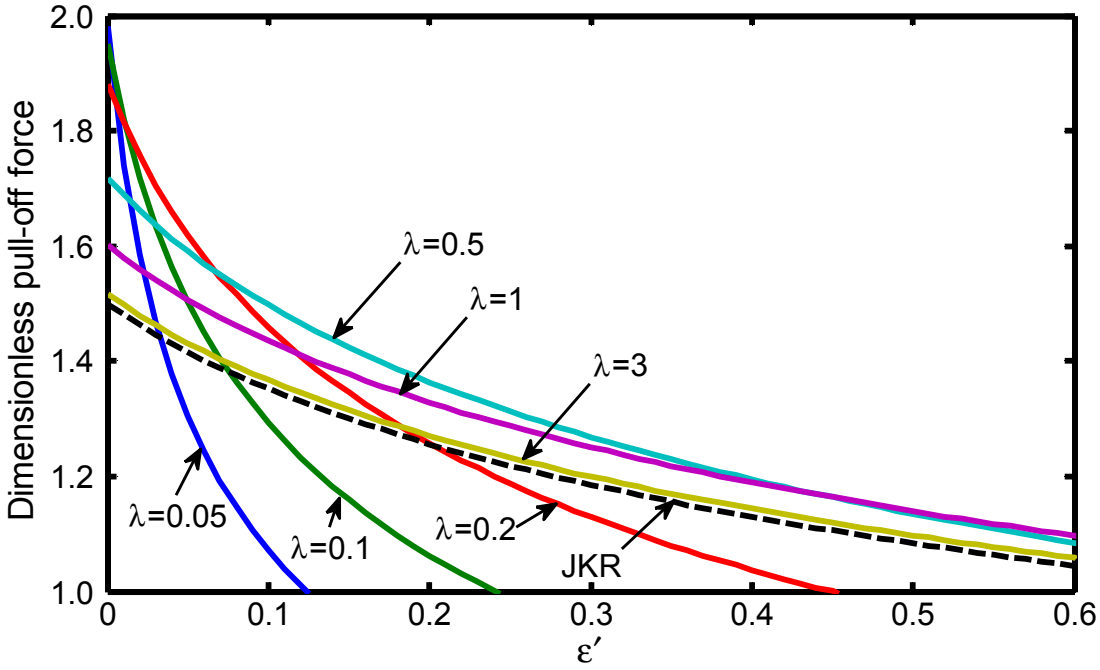

Figure 13b

Figures 13a and 13b Dimensionless pull-off force vs. ε' for a surface profile described by a combination of second- and fourth-order terms at different values of λ. The dashed curve represents the dimensionless pull-off force vs. ε' obtained by the extended JKR model for a surface profile described by a combination of second- and fourth-order terms.

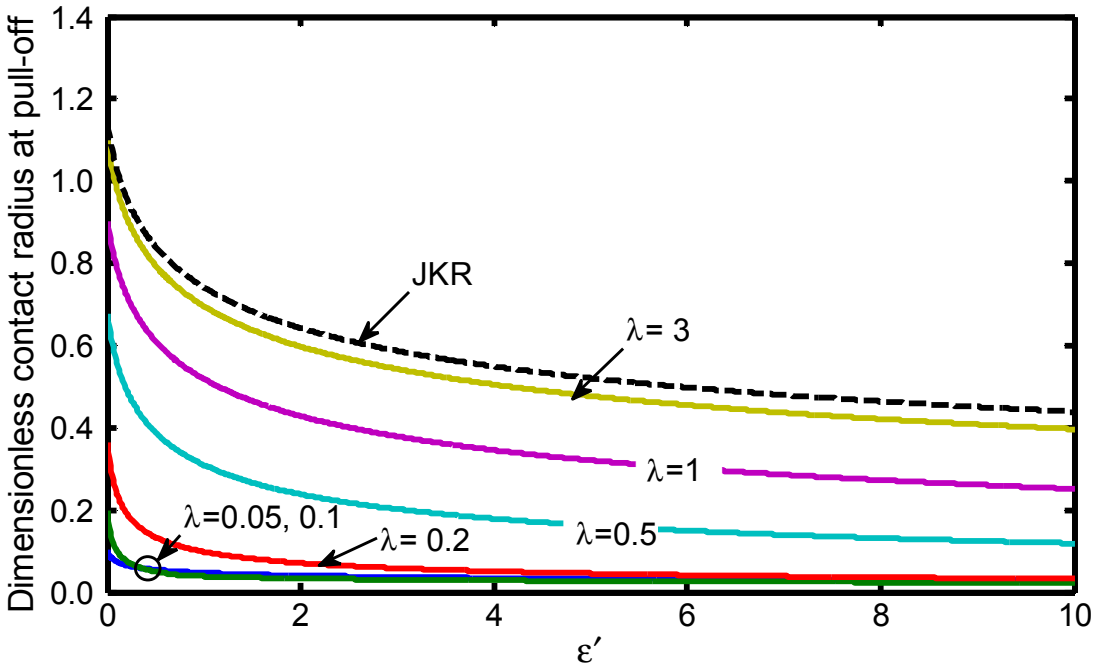

Figure 14 Dimensionless contact radius at pull-off vs. ε' for a surface profile described by a combination of second- and fourth-order terms at different values of λ. The dashed curve represents the dimensionless contact radius at pull-off vs. ε' obtained by the extended JKR model for a surface profile described by a combination of second- and fourth-order terms.

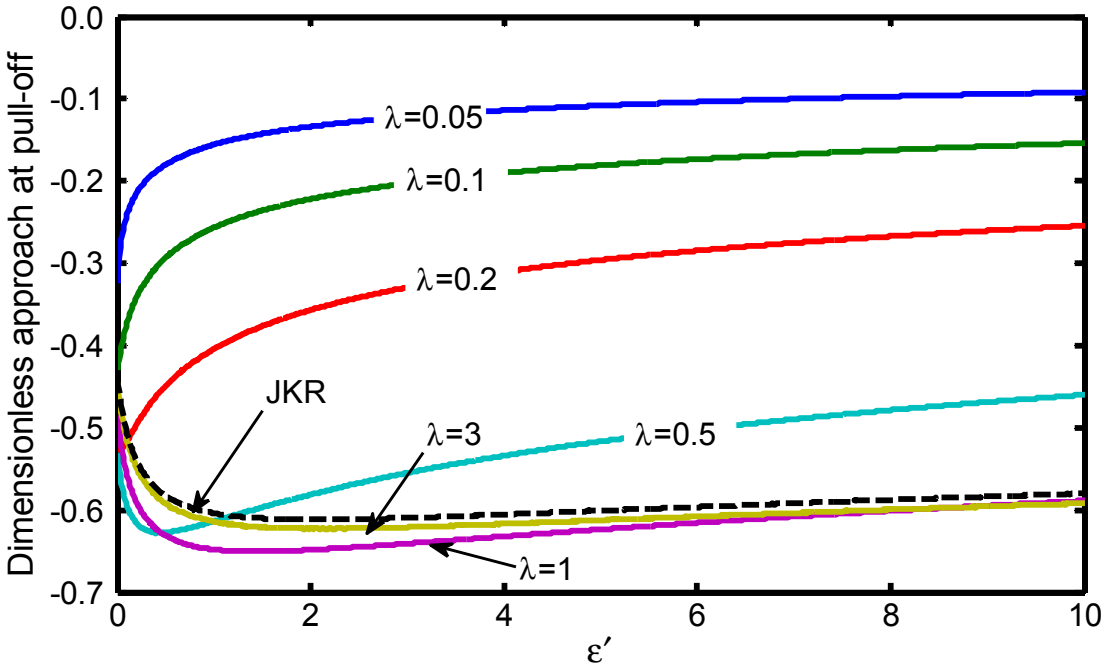

Figure 15 Dimensionless approach at pull-off vs. ε' for a surface profile described by a combination of second- and fourth-order terms at different values of λ. The dashed curve represents the dimensionless approach at pull-off force vs. ε' obtained by the extended JKR model for a surface profile described by a combination of second- and fourth-order terms.